Journal of the Mechanics and Physics of Solids 106 (2017) 60–79

Contents lists available at ScienceDirect

Journal of the Mechanics and Physics of Solids

journal homepage: www.elsevier.com/locate/jmps

A family of hyperelastic models for human brain tissue

L. Angela Mihai[a], Silvia Budday[b], Gerhard A. Holzapfel[c,d], Ellen Kuhl[e], Alain Goriely[f,*]

[a] School of Mathematics, Cardiff University, Cardiff, UK
[b] Lehrstuhl für Technische Mechanik, University of Erlangen-Nüremberg, Erlangen, Germany
[c] Institute of Biomechanics, Graz University of Technology, Graz, Austria
[d] Norwegian University of Science and Technology (NTNU), Faculty of Engineering Science and Technology, Trondheim, Norway
[e] Department of Mechanical Engineering, Stanford University, Stanford, USA
[f] Mathematical Institute, University of Oxford, Oxford, UK

ARTICLE INFO

Article history:
Received 6 April 2017
Revised 12 May 2017
Accepted 27 May 2017
Available online 31 May 2017

Keywords:
Brain mechanics
Hyperelasticity
Large deformations
Combined loading
Constitutive modeling

ABSTRACT

Experiments on brain samples under multiaxial loading have shown that human brain tissue is both extremely soft when compared to other biological tissues and characterized by a peculiar elastic response under combined shear and compression/tension: there is a significant increase in shear stress with increasing axial compression compared to a moderate increase with increasing axial tension. Recent studies have revealed that many widely used constitutive models for soft biological tissues fail to capture this characteristic response. Here, guided by experiments of human brain tissue, we develop a family of modeling approaches that capture the elasticity of brain tissue under varying simple shear superposed on varying axial stretch by exploiting key observations about the behavior of the nonlinear shear modulus, which can be obtained directly from the experimental data.

What we know to be true and what we believe to be reasonable for one or another real material serve as our guides in choosing different forms of constitutive equations. – Clifford Truesdell (1966).

1. Introduction

The study of the mechanical response of biological systems within a continuum framework relies on constitutive equations relating stresses to strains (Holzapfel, 2000). In the absence of a method to derive these constitutive equations from first principles, phenomenological models are routinely used. In particular, when a system behaves in the elastic regime, classes of hyperelastic models have been proposed for many tissues and organs. Ideally, these models are systematically calibrated and validated on multiaxial loading data (Misra et al., 2010; Sommer et al., 2013). Rather than using brute force and fit data to arbitrary strain-energy functions, it is well understood that a key element of constitutive modeling is to consider families of models with desirable properties. For instance, collagen-rich soft tissues are known to be mostly incompressible and display strong strain-stiffening response. Therefore, most of the current models for these tissues start with a functional form that both enforces these particular properties and is general enough to be adapted for specific systems.

* Corresponding author.
E-mail addresses: MihaiLA@cardiff.ac.uk (L.A. Mihai), silvia.budday@ltm.uni-erlangen.de (S. Budday), holzapfel@tugraz.at (G.A. Holzapfel), ekuhl@stanford.edu (E. Kuhl), goriely@maths.ox.ac.uk (A. Goriely).

http://dx.doi.org/10.1016/j.jmps.2017.05.015
0022-5096/

Brain tissue is strikingly different from most soft biological tissues: its microstructure is not governed by collagen and elastin fibers, which implies that brain typically lacks the characteristic strain-stiffening behavior of arteries, skeletal and cardiac muscle, or skin (Goriely et al., 2015a; 2015b). The typical behavior of these tissues, captured by models such as Fung's or Gent's (Horgan and Saccomandi, 2003), is that a strong stiffening is obtained at finite extension leading either to a singular limit (in the case of the Gent model) or exponential behavior (for the Fung model). Data analyses shows that these models are not suitable for brain tissue (Mihai et al., 2015). A natural problem is then to understand the defining characteristics of brain tissue and to identify a suitable family of hyperelastic models with these characteristics. Moreover, a model for brain tissue needs to be suitable for small to moderate strain as experienced in vivo (Bayly et al., 2006).

The analysis presented in this paper is based on the data of human brain tissues tested under finite uniaxial and multiaxial loading reported in Budday et al. (2017). In this article, the authors have established that the microstructural anisotropy due to the alignment of nerve fibers in the tissue does not result in an anisotropic elastic response similar to the effect of collagen fibers in other soft tissues. Therefore, we neglect a possible anisotropic response and assume here that brain tissue is isotropic. Another important consideration is the viscoelastic response of brain tissue. The data shows clearly that the response of brain tissue has a viscous component indicated by a different response in loading and unloading. However, in the first instance, we are interested in the tissue's effective elastic response under small strain rate. Following Budday et al. (2017), this response is obtained as the average between the loading and the unloading paths, assuming that this corresponds to the case when the strain rate approaches zero and the hysteresis vanishes. Therefore, for the rest of our analysis, we restrict our attention to isotropic elastic models.

In the elastic regime, recent experiments on brain tissues have further established another response under combined compression and shear, namely that the elastic shear stress increases sharply with increasing axial compression, while it only increases moderately with increasing tension (Budday et al., 2017; Levental et al., 2007; Mihai et al., 2015; Pogoda et al., 2014). From a modeling point of view, capturing this apparently contradictory behavior represents a major challenge. Similar behaviors were also observed in other soft tissues with large lipid content, such as adipose tissue (Mihai et al., 2015).

For brain and adipose tissues, Ogden-type hyperelastic incompressible isotropic models (Ogden, 1972) have been found in good agreement with the experimental data, both in single and multiaxial loading (Budday et al., 2017; Comley and Fleck, 2012; Destrade et al., 2015; Franceschini et al., 2006; Mihai et al., 2015; Miller and Chinzei, 1997; 2002; Moran et al., 2014; Nicolle et al., 2004; Prange and Margulies, 2002; Rashid et al., 2012; 2013; 2014), and the relative errors from their nonlinear least-squares fit to the experimental data suggest that the models with higher order terms are more successful in approximating the data than the ones with lower order terms. However, even though Ogden-type constitutive models are widely appealing since they are readily implemented in many popular software packages, the fact that a relatively large number of parameters may be required to approximate the data to the desired accuracy makes them less attractive to users.

Here, our objective is to build a family of isotropic hyperelastic strain-energy functions, with a small number of parameters, that exhibit the characteristic behavior under combined shear and compression or tension. To achieve this, we devise a systematic strategy to derive such models and demonstrate their performance on experimental data for human brain tissue from Budday et al. (2017). Our algorithmic approach is generic and, as such, applicable to other biological tissues with similar properties, including adipose tissue. We start our analysis in Section 2, with a detailed study of the deformation of a cuboid of isotropic hyperelastic material under simple shear superposed on finite axial stretch. This analysis reveals the crucial role of the nonlinear shear modulus defined as the ratio between the shear stress and the shear strain. Unlike the linear shear modulus which is a constant, in general, the nonlinear shear modulus is a function of the deformation that enables us to identify characteristic behaviors under large shear superposed on large compression or tension. In Section 3, we show that, for a given shear superposed on finite compression or tension, the elastic behavior under large shear is consistent with that under small shear. This observation is used to identify a generic strain-energy function capable of predicting the physical behavior of human brain tissues subjected to combined shear and tension or compression. In Sections 4 and 5, we exploit our key observations from the experimental data and employ the nonlinear shear modulus to derive a family of hyperelastic models with a small number of parameters that predict the elastic behavior of brain tissue under combined shear and axial loading and are suitable for finite-element analyses.

2. Finite shear superposed on axial stretch

The finite elastic deformation of a material body is described by the mapping $\mathbf{x} = \boldsymbol{\chi}(\mathbf{X})$, which defines a one-to-one correspondence between the positions of material points in the reference configuration $\mathbf{X} = (X, Y, Z) \in \mathcal{B}_0$ and their positions in the current configuration $\mathbf{x} = (x, y, z) \in \mathcal{B}$. Kinematics quantities for the deformation (Beatty, 1996; Truesdell and Noll, 2004) are associated with the deformation gradient

$$\mathbf{F} = \operatorname{Grad} \boldsymbol{\chi}. \tag{1}$$

Here, we restrict our attention to hyperelastic isotropic materials. These materials are described by a strain-energy function $\mathcal{W}(\lambda_1, \lambda_2, \lambda_3)$, where $\{\lambda_i\}_{i=1,2,3}$ are the principal stretches (Ogden, 1997, p. 94). We assume that the material is incompressible so that $J = \det \mathbf{F} = \lambda_1\lambda_2\lambda_3 = 1$. Then, the Cauchy stress tensor has the representation:

$$\boldsymbol{\sigma} = -p\mathbf{I} + \beta_1\mathbf{B} + \beta_{-1}\mathbf{B}^{-1}, \tag{2}$$

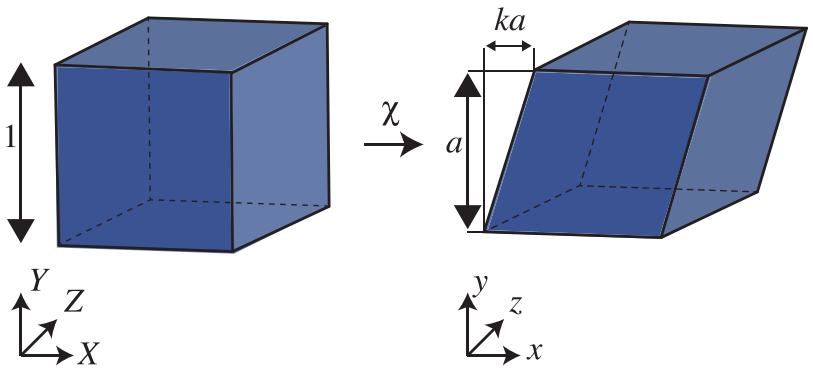

Fig. 1. Cuboid (left) deformed by simple shear superposed on axial stretch (right).

where $\mathbf{I}$ is the identity tensor, $\mathbf{B}=\mathbf{F}\cdot\mathbf{F}^{\mathrm{T}}$ is the left Cauchy–Green tensor, p is the Lagrange multiplier associated with the incompressibility constraint $J=1$, and

$$\begin{aligned}\beta_1&=\frac{1}{\lambda_1^2-\lambda_2^2}\left(\frac{\lambda_1^2+\lambda_3^2}{\lambda_1}\frac{\partial\mathcal{W}}{\partial\lambda_1}-\frac{\lambda_2^2+\lambda_3^2}{\lambda_2}\frac{\partial\mathcal{W}}{\partial\lambda_2}\right),\\ \beta_{-1}&=\frac{1}{\lambda_1^2-\lambda_2^2}\left(\frac{1}{\lambda_1}\frac{\partial\mathcal{W}}{\partial\lambda_1}-\frac{1}{\lambda_2}\frac{\partial\mathcal{W}}{\partial\lambda_2}\right),\end{aligned}\tag{3}$$

are the constitutive coefficients.

We consider an elastic cuboid deformed by simple shear superposed on axial stretch. This idealized deformation has been first proposed by Rajagopal and Wineman (1987) and used both to study the Poynting effect and to fit experimental data (Budday et al., 2017; Destrade et al., 2012; Mihai et al., 2015; Mihai and Goriely, 2011; 2013). In Cartesian coordinates, it reads

$$x=\frac{X}{\sqrt{a}}+kaY,\qquad y=aY,\qquad z=\frac{Z}{\sqrt{a}},\tag{4}$$

where (X, Y, Z) and (x, y, z) are the coordinates of the reference and current configurations, respectively (see Fig. 1). The deformation gradient for this deformation is

$$[\mathbf{F}]=\begin{bmatrix}1/\sqrt{a} & ka & 0\\ 0 & a & 0\\ 0 & 0 & 1/\sqrt{a}\end{bmatrix},\tag{5}$$

where $a>0$ is the (constant) *axial stretch*, $(a-1)$ is the *axial strain*, $k>0$ is the *shear parameter*, and $ka>0$ is the *shear strain*.

The corresponding left Cauchy–Green deformation tensor takes the form

$$[\mathbf{B}]=\begin{bmatrix}1/a+k^2a^2 & ka^2 & 0\\ ka^2 & a^2 & 0\\ 0 & 0 & 1/a\end{bmatrix},\tag{6}$$

with the eigenvalues

$$\begin{aligned}\lambda_1^2&=\frac{1+a^3\left(1+k^2\right)+\sqrt{\left[1+a^3\left(1+k^2\right)\right]^2-4a^3}}{2a}=\lambda^2,\\ \lambda_2^2&=\frac{1+a^3\left(1+k^2\right)-\sqrt{\left[1+a^3\left(1+k^2\right)\right]^2-4a^3}}{2a}=a\lambda^{-2},\\ \lambda_3^2&=\frac{1}{a}.\end{aligned}\tag{7}$$

The principal invariants of the tensor $\mathbf{B}$ in (6) are

$$\begin{aligned}I_1&=\mathrm{tr}\ (\mathbf{B})=a^2\left(1+k^2\right)+\frac{2}{a}=\lambda_1^2+\lambda_2^2+\lambda_3^2,\\ I_2&=\frac{1}{2}\left[(\mathrm{tr}\,\mathbf{B})^2-\mathrm{tr}\left(\mathbf{B}^2\right)\right]=a\left(2+k^2\right)+\frac{1}{a^2}=\lambda_1^2\lambda_2^2+\lambda_2^2\lambda_3^2+\lambda_3^2\lambda_1^2,\\ I_3&=\det\mathbf{B}=1=\lambda_1^2\lambda_2^2\lambda_3^2.\end{aligned}\tag{8}$$

We note that we can rewrite the second invariant as $I_2 = \lambda_1^{-2} + \lambda_2^{-2} + \lambda_3^{-2}$. The non-zero components of the associated Cauchy stress (2) are

$$\begin{aligned}
\sigma_{xx} &= \sigma_{zz} + \beta_1 k^2 a^2,\\
\sigma_{yy} &= \sigma_{zz} + \left(a^2 - \frac{1}{a}\right)\left(\beta_1 - \frac{\beta_{-1}}{a}\right) + \beta_{-1} k^2 a,\\
\sigma_{zz} &= -p + \frac{\beta_1}{a} + a\beta_{-1},\\
\sigma_{xy} &= ka^2\left(\beta_1 - \frac{\beta_{-1}}{a}\right),
\end{aligned} \tag{9}$$

and the principal stresses are given by (Truesdell and Noll, 2004, p. 143)

$$\sigma_i = \lambda_i \frac{\partial \mathcal{W}}{\partial \lambda_i} - p, \qquad i = 1, 2, 3. \tag{10}$$

A convenient way to quantify the shear response of a material under shear stress is to introduce the following *nonlinear shear modulus* (Truesdell and Noll, 2004, p. 174-175)

$$\mu = \frac{\sigma_1 - \sigma_2}{\lambda_1^2 - \lambda_2^2} = \frac{1}{\lambda_1^2 - \lambda_2^2}\left(\lambda_1 \frac{\partial \mathcal{W}}{\partial \lambda_1} - \lambda_2 \frac{\partial \mathcal{W}}{\partial \lambda_2}\right). \tag{11}$$

This modulus is a function of the deformation. In our case, it can be parameterized in terms of the axial stretch a and the shear parameter k as $\mu = \mu(a, k)$. Equivalently, the nonlinear shear modulus can be written in terms of the constitutive coefficients, using (3), as

$$\mu(a, k) = \beta_1 - \frac{\beta_{-1}}{a}. \tag{12}$$

It is easier in experiments to measure the components of the first Piola–Kirchhoff stress defined as the force per unit area in the reference configuration (Truesdell and Noll, 2004, pp. 124-125)

$$\mathbf{P} = (\det \mathbf{F})\, \boldsymbol{\sigma} \cdot \mathbf{F}^{-\mathrm{T}}. \tag{13}$$

Since the shear component of the first Piola–Kirchhoff stress tensor $P_{xy} = \sigma_{xy}\, a$ is proportional to the shear strain ka, the *nonlinear shear modulus* (11), or equivalently (12), is simply the ratio between the elastic shear stress P_{xy} and the shear strain ka, i.e.,

$$\mu(a, k) = \frac{\sigma_{xy}}{ka^2} = \frac{P_{xy}}{ka}. \tag{14}$$

Hence the nonlinear shear modulus defined here can be obtained directly from the experimental measurements.

There are two interesting limits of the nonlinear shear modulus. First, when the axial stretch a is finite and the shear strain is small, i.e., for infinitesimal simple shear superposed on finite axial stretch, the nonlinear shear modulus (11) converges to

$$\widetilde{\mu}(a) = \lim_{k \to 0} \mu(a, k). \tag{15}$$

Second, in the linear elastic limit, the nonlinear shear modulus (11) converges to the well-known linear shear modulus μ_0 of the infinitesimal theory,

$$\mu_0 = \lim_{a \to 1}\left(\lim_{k \to 0} \mu(a, k)\right) = \lim_{a \to 1} \widetilde{\mu}(a). \tag{16}$$

3. Modeling strategy

Our objective is to identify a strain-energy function that can predict the physical behavior of human brain tissues subjected to combined shear and tension or compression. The experimental setup is described in detail in Budday et al. (2017) and summarized in Appendix A, and the deformation attained is idealised by the homogeneous deformation (4). Note that obtaining ideal homogeneous deformations with very soft samples is known to be challenging as ideal frictionless boundary conditions are difficult to achieve and barrelling may occur in compression. However, it remains our main theoretical tool in an attempt to organise the data. Accordingly, for a fixed axial stretch a and shear parameter k, we measure the shear component P_{xy} of the first Piola–Kirchhoff stress tensor and calculate the corresponding nonlinear shear modulus μ using Eq. (14).

Fig. 2 summarizes the nonlinear shear modulus $\mu(a, k)$ extracted from the experimental data for human brain tissue tested under multiaxial loading conditions (Budday et al., 2017) (see Appendix A). Two interesting characteristics emerge from these figures. First, in Fig. 2A, we observe that the variation of the nonlinear shear modulus with respect to the shear

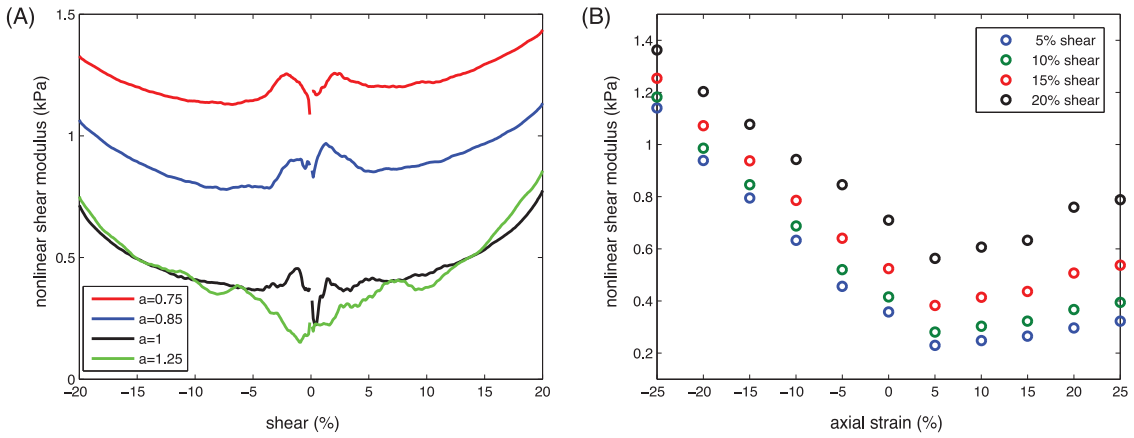

Fig. 2. Nonlinear shear modulus given by the experimental measurements for brain tissue (A) under simple shear superposed on axial tension or compression, and (B) under varying compression and tension levels evaluated at different levels of shear. As the experiments suggest, the nonlinear shear modulus at any fixed shear increases significantly with increasing compression and remains almost constant or increases moderately with increasing tension. Here and in all the following figures the axial strain is $(a-1)$.

parameter is similar for different values of fixed stretches, up to global vertical shift. Indeed, the different curves have the same qualitative characteristics shape. Second, in Fig. 2B, we observe that, under large compressive loading, the nonlinear shear modulus increases sharply and almost linearly as the stretch parameter $0 < a < 1$ decreases, while under tension, the nonlinear shear modulus remains almost constant or increases moderately as the parameter $a > 1$ increases. Strikingly, although this behavior was observed before for small shear (Levental et al., 2007; Mihai et al., 2015; Pogoda et al., 2014), here we see that the behavior of the nonlinear shear modulus with respect to the stretch at finite fixed shear is similar to that under small shear.

3.1. Preliminary considerations

Our modeling strategy can accommodate various forms of strain-energy functions. Here, we consider the following Ogden-type model (Ogden, 1972), which will be useful in predicting the characteristic elastic behavior under simple shear superposed on finite axial stretch,

$$\mathcal{W}_{\rm og}(\lambda_1,\lambda_2,\lambda_3)=\frac{c_0(a)}{2\alpha(a)}\left(\lambda_1^{2\alpha(a)}+\lambda_2^{2\alpha(a)}+\lambda_3^{2\alpha(a)}-3\right). \tag{17}$$

We know from Budday et al. (2017) and Mihai et al. (2015) that Ogden models can capture the qualitative trend reported above. Indeed, for each prescribed stretch a, the particular model (17) captures our experimental data well if $c_0(a)$ and $\alpha(a)$ change with the stretch parameter a (Budday et al., 2017) (see Appendix B). For fixed a, the corresponding principal stresses take on the form

$$\sigma_i=c_0(a)\lambda_i^{2\alpha(a)}-p,\qquad i=1,2,3. \tag{18}$$

Then the nonlinear shear modulus (11) simplifies to

$$\mu(a,k)=c_0(a)\frac{\lambda_1^{2\alpha(a)}-\lambda_2^{2\alpha(a)}}{\lambda_1^2-\lambda_2^2}. \tag{19}$$

When the shear strain is small, the nonlinear shear modulus (23) converges to

$$\widetilde{\mu}(a)=\lim_{k\to 0}\mu(a,k)=c_0(a)\frac{a^{1-\alpha(a)}(1-a^{3\alpha(a)})}{1-a^3}. \tag{20}$$

In the linear elastic limit, this modulus becomes

$$\mu_0=\lim_{a\to 1}\widetilde{\mu}(a)=c_0(1)\alpha(1). \tag{21}$$

However, a constitutive model of the form (17) fails to simultaneously capture the constitutive response of brain tissue at different stretch levels when using the calibration approach tested in Budday et al. (2017) (see Appendix B). This suggests that either a different calibration strategy is required or a different constitutive model should be considered. We consider both approaches next. First, we develop a different calibration strategy. Second, we consider constitutive models with more parameters.

4. One-term (two-parameter) constitutive model

As shown in Fig. 2, for a given shear superposed on varying levels of tension and compression, the changes in the nonlinear shear modulus under large shear computed from the experimental data are consistent with those under small shear. In particular, this modulus increase sharply in compression as $0 < a < 1$ decreases, and remains almost constant or increase moderately in tension as $a > 1$ increases. Theoretically, we notice that, since in (17), the parameters $c_0(a)$ and $\alpha(a)$ depend only on the stretch a, constant values for these parameters can be obtained by calibrating to the corresponding experimental results the nonlinear shear modulus for small shear superposed on varying axial stretches a (20). Once the model parameters are found, they can be used to predict the nonlinear shear modulus (19), and hence the elastic behavior under large shear superposed on different axial deformations.

To obtain a hyperelastic model that captures the observed behavior of human brain tissue while keeping the number of model parameters low, we consider the one-term (two-parameter) Ogden model (17) with the strain-energy function

$$\mathcal{W}_0(\lambda_1,\lambda_2,\lambda_3)=\frac{c_0}{2\alpha}\left(\lambda_1^{2\alpha}+\lambda_2^{2\alpha}+\lambda_3^{2\alpha}-3\right), \tag{22}$$

where c_0 and α are constant parameters independent of the stretch value a. These model parameters can be found from the experimental data of human brain tissue under small shear superposed on varying axial stretches a, as in Mihai et al. (2015). Then the constitutive model (22) can be deformed by finite simple shear or by simple shear superposed on any finite axial stretch (4) with the shear parameter k and axial stretch a. In this case, c_0 and α are fixed material parameters, and the nonlinear shear modulus (19), the nonlinear shear modulus under small shear strain (20), and their linear elastic limit (21) take on the following explicit forms:

$$\mu(a,k)=c_0\frac{\lambda_1^{2\alpha}-\lambda_2^{2\alpha}}{\lambda_1^2-\lambda_2^2}, \tag{23}$$

$$\widetilde{\mu}(a)=\lim_{k\to 0}\mu(a,k)=c_0\frac{a^{1-\alpha}\left(1-a^{3\alpha}\right)}{1-a^3}, \tag{24}$$

$$\mu_0=\lim_{a\to 1}\widetilde{\mu}(a)=c_0\alpha. \tag{25}$$

4.1. Model calibration

In this section, we devise a two-step procedure to calibrate the strain-energy function (22) to the human brain experiments. The only experimental measurements that we require for the model calibration correspond to the nonlinear shear modulus for small shear superposed on varying axial deformations. To calibrate the constant parameters to the experimental data, we employ a nonlinear least squares procedure in Matlab, `lsqnonlin.m` (Budday et al., 2017; Mihai et al., 2015; Ogden et al., 2004). We then compare the predicted results with experimental data for finite simple shear superposed on axial tension or compression.

Step 1. (preliminary approximation of experimental data) First, we consider the experimental data for simple shear, up to 20%, and for simple shear superposed on any fixed axial stretch, up to 25% tension or compression (in 5% increments), and note that the available data are highly reliable at more than 5% shear, but contain some noise in the low shear range, at less than 5% in magnitude. To identify more reliable values everywhere, we calibrate the strain-energy function $\mathcal{W}_{\text{og}}$ of Eq. (17) to the experimental data for fixed axial stretch and finite simple shear by varying the parameters $c_0(a)$ and $\alpha(a)$ with the stretch parameter a. We can calibrate this model using the experimental data of human brain tissue for shear stress under simple shear superposed on a fixed axial stretch.

In Appendix B, we summarize the constitutive behavior of the calibrated model, which shows excellent agreement with the experimental results at more than 5% shear and offers reliable predictions of the elastic behavior at less than 5% shear. In particular, for each axial stretch a, the nonlinear shear modulus under small shear $\widetilde{\mu}(a)$ is given by (20) and the predicted values are denoted by $\widetilde{\mu}_{\text{data}}(a)$. In the linear elastic limit, the shear modulus (21) is equal to $\mu_0=0.3379$ kPa.

Step 2. (constitutive model calibration) Second, in order to accurately capture the behavior of the nonlinear shear modulus at different values of the axial stretch, we consider the hyperelastic model characterized by the strain-energy function $\mathcal{W}_0$ of Eq. (22). For this model, we calibrate the nonlinear shear modulus $\widetilde{\mu}(a)$ of Eq. (24) for small shear superposed on varying axial deformations, up to 25% tension or compression (in 5% increments), to the corresponding values identified from the experimental data at Step 1, $\widetilde{\mu}_{\text{data}}(a)$, and obtain the constant parameters $c_0=-0.0939$ kPa and $\alpha=-4.0250$. This calibration is illustrated in Fig. 3 together with the associated relative error $|P_{xy}^{\text{model}}-P_{xy}^{\text{data}}|/|P_{xy}^{\text{data}}|$, where P_{xy}^{model} and P_{xy}^{data} are the predicted and measured values of the shear stress, respectively, and $|\cdot|$ denotes the absolute value.

According to Eq. (25), the calibrated model predicts a linear shear modulus of $\mu_0=c_0\alpha=0.3779$ kPa and a Young's modulus of $E_0=3\mu_0=1.1338$ kPa, i.e., this model offers a very good approximation in the linear elastic regime, where a

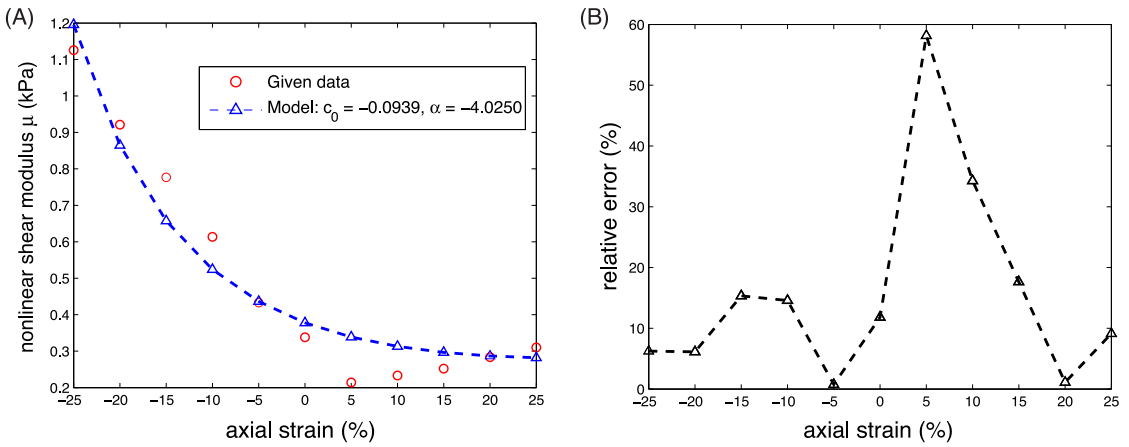

Fig. 3. Constitutive behavior of strain-energy function $\mathcal{W}_0 = c_0\left(\lambda_1^{2\alpha} + \lambda_2^{2\alpha} + \lambda_3^{2\alpha} - 3\right)/(2\alpha)$ with parameters $c_0 = -0.0939$ kPa and $\alpha = -4.0250$ under small shear superposed on varying axial tension or compression: (A) nonlinear shear modulus $\widetilde{\mu}$ versus axial strain, given data and model, and (B) associated relative error for the shear stress P_{xy}.

Table 1
Strain-energy function with related model parameters and calibrated values (and units) for human brain tissues.

strain-energy function	eq.	model	parameter	value	unit
$\mathcal{W}_0$	(22)	Ogden	c_0	−0.0939	kPa
			α	−4.0250	–
linear elastic limit	(25)	–	μ_0	0.3779	kPa

linear shear modulus $\mu_0 = 0.3379$ kPa was identified from the experimental data at Step 1 (see Appendix B). This is to be expected, since the model was calibrated to data for small shear deformations (Fig. 3). For comparison, a similar one-term (two-parameter) Ogden strain-energy function but a different calibration method, was used in Budday et al. (2017), and a shear modulus of $\mu_0 = 0.66$ kPa was found, but it was also noted that this value overestimates the stiffness under the linear elastic regime.

Table 1 summarizes the strain-energy function for the proposed model, its constant parameters, their calibrated values, and units. Fig. 4 shows the predicted shear stress P_{xy} and nonlinear shear modulus μ compared to the experimental data for simple shear, up to 20% shear strain, superposed on up to 25% compression or tension (in 5% increments), and the relative errors.

Remark 1. In the above calibration procedure, the preliminary Step 1, where reliable data for the nonlinear shear modulus under small shear deformations are identified, is performed only because the given experimental data are noisy in the small shear range, and more reliable values are required for the model calibration at Step 2. If reliable experimental data for the small shear deformations were provided directly, then Step 1 would not be necessary. At Step 2, the choice of the strain-energy function $\mathcal{W}_0$ is not restricted to the particular form suggested here, but our present choice was guided by the fact that we wanted to keep the number of constant model parameters low. Moreover, although the approximation under small shear superposed on varying axial stretch in Fig. 3 can be improved, as shown in Appendix C, under large shear deformations, the results remain similar. This is due to the fact that, as shown in Fig. 2B, if compression increases, then the nonlinear elastic modulus increases slower under larger shear, but if tension increases, then the rate of increase in this modulus remains virtually the same for different levels of shear.

5. Three-term (four-parameter) constitutive model

In this section, we construct a strain-energy function that matches the observed behaviors of human brain tissue under simple shear superposed on finite axial stretch by combining the Mooney–Rivlin model (Mooney, 1940; Rivlin, 1948)

$$\mathcal{W}_{\rm mr}(\lambda_1, \lambda_2, \lambda_3) = \frac{c_1}{2}\left(\lambda_1^2 + \lambda_2^2 + \lambda_3^2 - 3\right) + \frac{c_2}{2}\left(\lambda_1^{-2} + \lambda_2^{-2} + \lambda_3^{-2} - 3\right), \tag{26}$$

where c_1 and c_2 are two constant parameters, with the one-term Ogden model (17). The Mooney–Rivlin model has the property that its nonlinear shear modulus depends only on a, i.e.,

$$\mu(a, k) = \widetilde{\mu}(a) = c_1 + \frac{c_2}{a}. \tag{27}$$

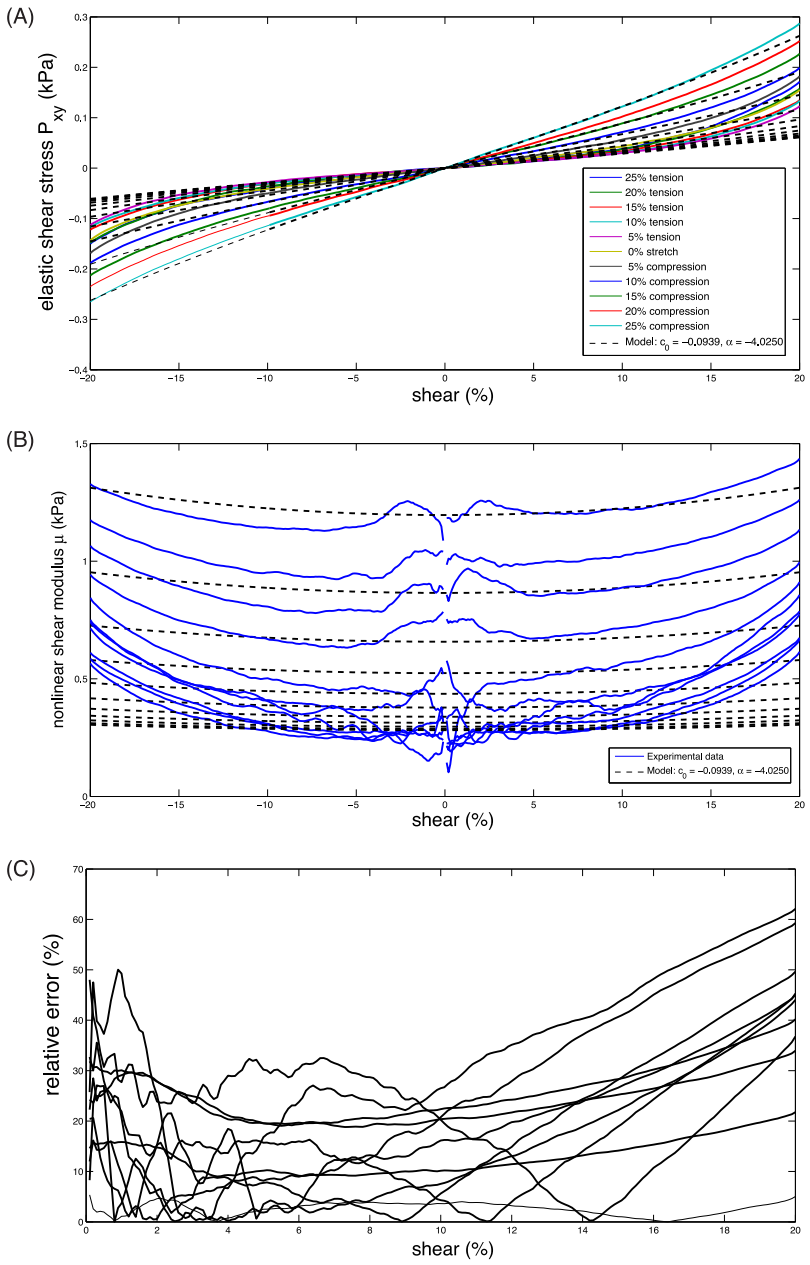

Fig. 4. Constitutive behavior of strain-energy function $\mathcal{W}_0 = c_0\left(\lambda_1^{2\alpha} + \lambda_2^{2\alpha} + \lambda_3^{2\alpha} - 3\right)/(2\alpha)$ with parameters $c_0 = -0.0939$ kPa and $\alpha = -4.0250$ under simple shear superposed on different levels of axial tension or compression: (A) shear stress P_{xy} versus shear strain, experiment and model, (B) nonlinear shear modulus μ versus axial strain, experiment and model, and (C) associated relative error for the shear stress P_{xy}. The corresponding linear shear modulus is $\mu_0 = 0.3779$ kPa.

Moreover, for this model, suitable values for the constant parameters can be found such that the nonlinear shear modulus increases linearly as the stretch parameter $0 < a < 1$ decreases, and remains almost constant as the parameter $a > 1$ increases, as shown in Mihai et al. (2015). These particular characteristics of the Mooney–Rivlin model will be useful when approximating the stress-strain curves in Fig. 2A, which are only translated vertically while their shape appears is almost invariant under variations of the stretch values a. To construct the strain-energy function for the constitutive model, we devise the following three-step procedure:

Step 1. We begin with a three-term (four-parameter) Ogden model by additively combining the strain-energy functions (17) and (26),

$$\mathcal{W}_1(\lambda_1,\lambda_2,\lambda_3)=\frac{c_0}{2\alpha}\left(\lambda_1^{2\alpha}+\lambda_2^{2\alpha}+\lambda_3^{2\alpha}-3\right)+\frac{c_1}{2}\left(\lambda_1^{2}+\lambda_2^{2}+\lambda_3^{2}-3\right)+\frac{c_2}{2}\left(\lambda_1^{-2}+\lambda_2^{-2}+\lambda_3^{-2}-3\right), \tag{28}$$

where c_0, α, c_1, and c_2 are constant material parameters. To calibrate this model, we use the experimental data of human brain tissue for shear stress under simple shear superposed on a fixed axial stretch, as in Budday et al. (2017), i.e., by fixing a in the deformation gradient (5). Then the constitutive model (28) can be deformed by simple shear or by simple shear superposed on any axial stretch (4) with the shear parameter k and axial stretch a. Since c_0, α, c_1, and c_2 are fixed material parameters, the nonlinear shear modulus (11) and the nonlinear shear modulus under small shear strain (15) take on the following explicit forms

$$\mu_1(a,k)=c_0\frac{\lambda_1^{2\alpha}-\lambda_2^{2\alpha}}{\lambda_1^{2}-\lambda_2^{2}}+c_1+\frac{c_2}{a}, \tag{29}$$

$$\widetilde{\mu}_1(a)=\lim_{k\to 0}\mu_1(a,k)=c_0\frac{a^{1-\alpha}\left(1-a^{3\alpha}\right)}{1-a^3}+c_1+\frac{c_2}{a}. \tag{30}$$

Step 2. Next, in order to approximate the nonlinear shear modulus at different values of the axial stretch while preserving the changes with shear from the previous step (as shown in Fig. 2A), we augment the strain-energy function $\mathcal{W}_1$ of (28) by a correction function $\mathcal{W}_2$ to obtain an isotropic hyperelastic model of the form

$$\mathcal{W}(\lambda_1,\lambda_2,\lambda_3)=\mathcal{W}_1(\lambda_1,\lambda_2,\lambda_3)+\mathcal{W}_2(\lambda_1,\lambda_2,\lambda_3). \tag{31}$$

For the hyperelastic model (31), the nonlinear shear modulus (11) is simply the sum of the nonlinear shear moduli of both functions, i.e.,

$$\mu=\frac{1}{\lambda_1^2-\lambda_2^2}\left(\lambda_1\frac{\partial\mathcal{W}}{\partial\lambda_1}-\lambda_2\frac{\partial\mathcal{W}}{\partial\lambda_2}\right)=\mu_1+\mu_2. \tag{32}$$

where μ_1 is the nonlinear shear modulus (29) of the strain-energy function $\mathcal{W}_1$, given by (28), and μ_2 is the nonlinear shear modulus of the correction function $\mathcal{W}_2$ which needs to be determined. Motivated by our experimental observations, the nonlinear shear modulus μ given by (32) must increase sharply in compression as $0<a<1$ decreases, and remain almost constant or increase moderately in tension as $a>1$ increases (see Fig. 2). To satisfy these conditions, we look for a nonlinear shear modulus correction $\mu_2(a,k)=\widetilde{\mu}_2(a)$, varying only with the stretch parameter a. Since the Mooney–Rivlin model is the only prominent model that satisfies this condition, we consider

$$\mathcal{W}_2(\lambda_1,\lambda_2,\lambda_3)=\frac{b_1}{2}\left(\lambda_1^{2}+\lambda_2^{2}+\lambda_3^{2}-3\right)+\frac{b_2}{2}\left(\lambda_1^{-2}+\lambda_2^{-2}+\lambda_3^{-2}-3\right), \tag{33}$$

with the nonlinear shear modulus

$$\mu_2=b_1+\frac{b_2}{a}. \tag{34}$$

In terms of the nonlinear shear modulus of the functions $\mathcal{W}_1$ and $\mathcal{W}_2$, we have

$$\mu_2=\widetilde{\mu}(a)-\widetilde{\mu}_1(a), \tag{35}$$

where $\widetilde{\mu}_1(a)$ is given by (30) and $\widetilde{\mu}(a)=\lim_{k\to 0}\mu$, with μ defined by (32). Therefore, the constants b_1 and b_2 can be found by calibrating (34) to the known values $\widetilde{\mu}_{\text{data}}(a)-\widetilde{\mu}_1(a)$, where $\widetilde{\mu}_{\text{data}}(a)$ are the values of the nonlinear shear modulus at small shear strain identified from the experimental data as shown in Appendix B.

Step 3. The resulting hyperelastic model (31) then consists of the free energy function $\mathcal{W}_1$ and the correction function $\mathcal{W}_2$. The final model takes on the form

$$\begin{aligned}\mathcal{W}(\lambda_1,\lambda_2,\lambda_3)=&\frac{c_0}{2\alpha}\left(\lambda_1^{2\alpha}+\lambda_2^{2\alpha}+\lambda_3^{2\alpha}-3\right)\\&+\frac{\bar{c}_1}{2}\left(\lambda_1^{2}+\lambda_2^{2}+\lambda_3^{2}-3\right)+\frac{\bar{c}_2}{2}\left(\lambda_1^{-2}+\lambda_2^{-2}+\lambda_3^{-2}-3\right),\end{aligned} \tag{36}$$

in terms of four global parameters. The corresponding nonlinear shear modulus (11), the nonlinear shear modulus under small shear strain (15), and their linear elastic limit (16) are, respectively,

$$\mu(a,k)=c_0\frac{\lambda_1^{2\alpha}-\lambda_2^{2\alpha}}{\lambda_1^{2}-\lambda_2^{2}}++\bar{c}_1+\frac{\bar{c}_2}{a}, \tag{37}$$

$$\widetilde{\mu}(a)=\lim_{k\to 0}\mu(a,k)=c_0\frac{a^{1-\alpha}\left(1-a^{3\alpha}\right)}{1-a^3}+\bar{c}_1+\frac{\bar{c}_2}{a}, \tag{38}$$

$$\mu_0=\lim_{a\to 1}\widetilde{\mu}(a)=c_0\alpha+\bar{c}_1+\bar{c}_2. \tag{39}$$

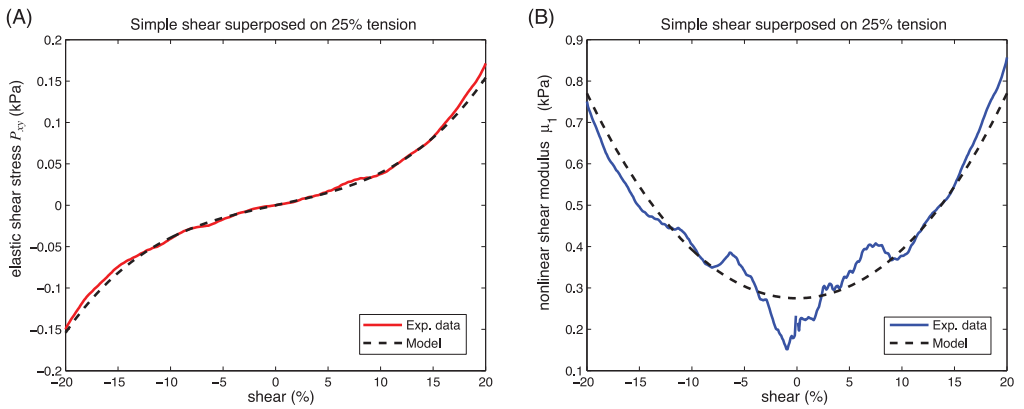

Fig. 5. Constitutive behavior of strain-energy function $\mathcal{W}_1$ under simple shear superposed on 25% axial tension, in Step 1: (A) shear stress P_{xy} versus shear strain, experiment and model with parameters $c_0 = 0.0653$ kPa, $\alpha = 7.1813$, $c_1 = -0.2302$ kPa, and $c_2 = -1.9842$ kPa, and (B) nonlinear shear modulus μ_1 versus shear strain, experiment and model.

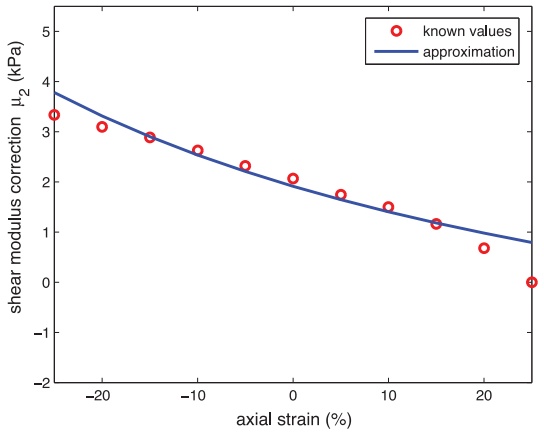

Fig. 6. Constitutive behavior of strain-energy function $\mathcal{W}_2$ in Step 2: nonlinear shear modulus correction μ_2 versus compression or tension, experiment and model with parameters $b_1 = -3.5899$ kPa and $b_2 = 5.5218$ kPa.

5.1. Model calibration

Next, we calibrate the model (36) to the human brain experiments (see Appendix A). At Step 1, the only experimental measurement we need to calibrate the model is the shear stress under simple shear superposed on a chosen axial stretch (see Appendix B). At Step 2, we require the nonlinear shear modulus under small shear superposed on varying compression or tension deformations. We then compare the predicted results for the shear stress and nonlinear shear modulus with experimental data for simple shear superposed on different axial deformations.

Step 1. (constitutive model initial calibration) First, we consider the experimental data for simple shear, up to 20%, superposed on 25% tension. Note that, in Fig. 2, the nonlinear shear modulus at 25% tension is almost equal to that under simple shear. In Fig. 5A, we calibrate the shear stress for the model $\mathcal{W}_1$ in (28) to these data and obtain $c_0 = 0.0653$ kPa, $\alpha = 7.1813$, $c_1 = -0.2302$ kPa, and $c_2 = -1.9842$ kPa. In Fig. 5B, the associated nonlinear shear modulus μ_1 of Eq. (29) is compared to the nonlinear shear modulus computed from the experimental data.

Step 2. (calibration correction) Second, from each experimental data set for the shear stress at different axial deformations, up to 25% compression or tension (in 5% increments), we evaluate the function (28) and its nonlinear shear modulus (30) and identify the nonlinear shear modulus values $\widetilde{\mu}_{\text{data}}(a)$ at small shear as explained in Appendix B. We then calibrate the nonlinear shear modulus correction μ_2 of Eq. (34) to the known values $\widetilde{\mu}_{\text{data}}(a) - \widetilde{\mu}_1(a)$, where $\widetilde{\mu}_1(a)$ is given by Eq. (30), and obtain $b_1 = -3.5899$ kPa and $b_2 = 5.5218$ kPa, as shown in Fig. 6.

Step 3. (constitutive model) The final hyperelastic model is then given by the strain-energy function $\mathcal{W} = \mathcal{W}_1 + \mathcal{W}_2$ of Eq. (36), i.e., the sum of the two models, with parameter values of $c_0 = 0.0653$ kPa, $\alpha = 7.1813$, $\bar{c}_1 = c_1 + b_1 = -3.8201$ kPa, and

Table 2
Strain-energy functions with related model parameters and calibrated values (and units) for human brain tissues.

step	strain energy	eq.	model	parameter	value	unit
Step 1	$\mathcal{W}_1$	(28)	Ogden	c_0	0.0653	kPa
				α	7.1813	–
				c_1	−0.2302	kPa
				c_2	−1.9842	kPa
Step 2	$\mathcal{W}_2$	(33)	Mooney–Rivlin	b_1	−3.5899	kPa
				b_2	5.5218	kPa
Step 3	$\mathcal{W} = \mathcal{W}_1 + \mathcal{W}_2$	(36)	Ogden	c_0	0.0653	kPa
				α	7.1813	–
				$\bar{c}_1$	−3.8201	kPa
				$\bar{c}_2$	3.5376	kPa
–	–	(39)	linear elastic limit	μ_0	0.1864	kPa

$\bar{c}_2 = c_2 + b_2 = 3.5376$ kPa. According to Eq. (39), the proposed model predicts a linear shear modulus of $\mu_0 = c_0\alpha + \bar{c}_1 + \bar{c}_2 = 0.1864$ kPa, which corresponds to a Young's modulus of $E_0 = 3\mu_0 = 0.5593$ kPa. This estimate for the shear modulus is lower than the one obtained in Appendix B.

Table 2 summarizes the three steps, with the corresponding strain-energy functions, model parameters, calibrated values, and units. Fig. 7 compares the predicted shear stress P_{xy} and nonlinear shear modulus μ with the experimental data for simple shear, up to 20% shear strain, superposed on up to 15% compression or tension (in 5% increments), and shows the relative errors. At large shear strains, close to 20%, the relative errors in Fig. 7C are comparable with those in Fig. 4C.

Remark 2. Note that the overall model constructed here contains three terms with four parameters $c_0 = 0.0653$ kPa, $\alpha = 7.1813$, $\bar{c}_1 = -3.8201$, $\bar{c}_2 = 3.5376$, i.e., only four parameters are needed for the finite element implementation of this model.

6. Discussion

Understanding the constitutive behavior of human brain tissue is critically important to study its mechanical function, to evaluate the stresses that cannot be measured in vivo, and to predict its response to physiological and pathological loading. In spite of extensive research, we only now begin to understand that brain tissue belongs to a special class of soft tissues with unique and distinct constitutive properties. We typically associate soft tissues with a constitutive behavior that is primarily driven by the microstructure of their extracellular matrix with load bearing fibers of collagen and elastin. There is a general agreement to model this type of behavior with a strain-energy function supplemented by a strain-stiffening term that acts along the fiber direction. Probably the most prominent representative of this class of models is the Holzapfel–Gasser–Ogden model (Holzapfel et al., 2000), which is widely used to model various soft tissues including arteries, heart valve, cardiac muscle, ocular tissue. While earlier attempts have simply adapted this model to simulate brain tissue (Cloots et al., 2011), recent studies suggest that brain tissues behave inherently differently (see Appendix B). In particular, when brain tissue is subject to large strains, the shear modulus increases significantly under axial compression, but not under tension.

Experimental studies of human brain tissue have found that, in general, its behavior can reasonably be approximated by an Ogden-type model for nonlinear, incompressible, isotropic, rubber-like materials. Ogden models (Ogden, 1972) are widely used and are appealing for many reasons, not least because they are readily available in many commercial software packages. In fact, the Ogden model outperforms many other commonly used models including the Neo–Hookean, Mooney–Rivlin, Fung, and Gent models when modeling human (Budday et al., 2017) and murine (Mihai et al., 2015) brain tissue and fat under multiaxial loading. Our recent studies further reveal that, under combined finite shear and axial deformation, human brain tissue displays a pronounced tension-compression asymmetry, which manifests though a significant increase in shear stress with increasing axial compression compared to a moderate increase with increasing axial tension (Budday et al., 2017). Similarly, in murine brain tissue under small shear, the nonlinear shear modulus increases with increasing axial compression but remains almost constant with increasing axial tension (Mihai et al., 2015; Pogoda et al., 2014). By neglecting time-dependent material effects, such as viscoelasticity (de Rooij and Kuhl, 2016) or poroelasticity (Franceschini et al., 2006), and focusing exclusively on the quasi-time-independent elastic behavior, in Budday et al. (2017), it is shown that, at fixed axial stretch, the one-term Ogden model performs well and captures accurately the variation of stress with respect to large shear. However, as axial stretch is varied, the two parameters change considerably. Hence, either a different model or a different calibration strategy is required under multiaxial loading. The experimental data shows that, for a given shear superposed on varying levels of tension and compression, the changes in the nonlinear shear modulus under large shear are qualitatively similar to those under small shear. Furthermore, in view of the many typical difficulties which arise from the numerical least-squares approximation of large experimental data sets, such as non-uniqueness of approximate

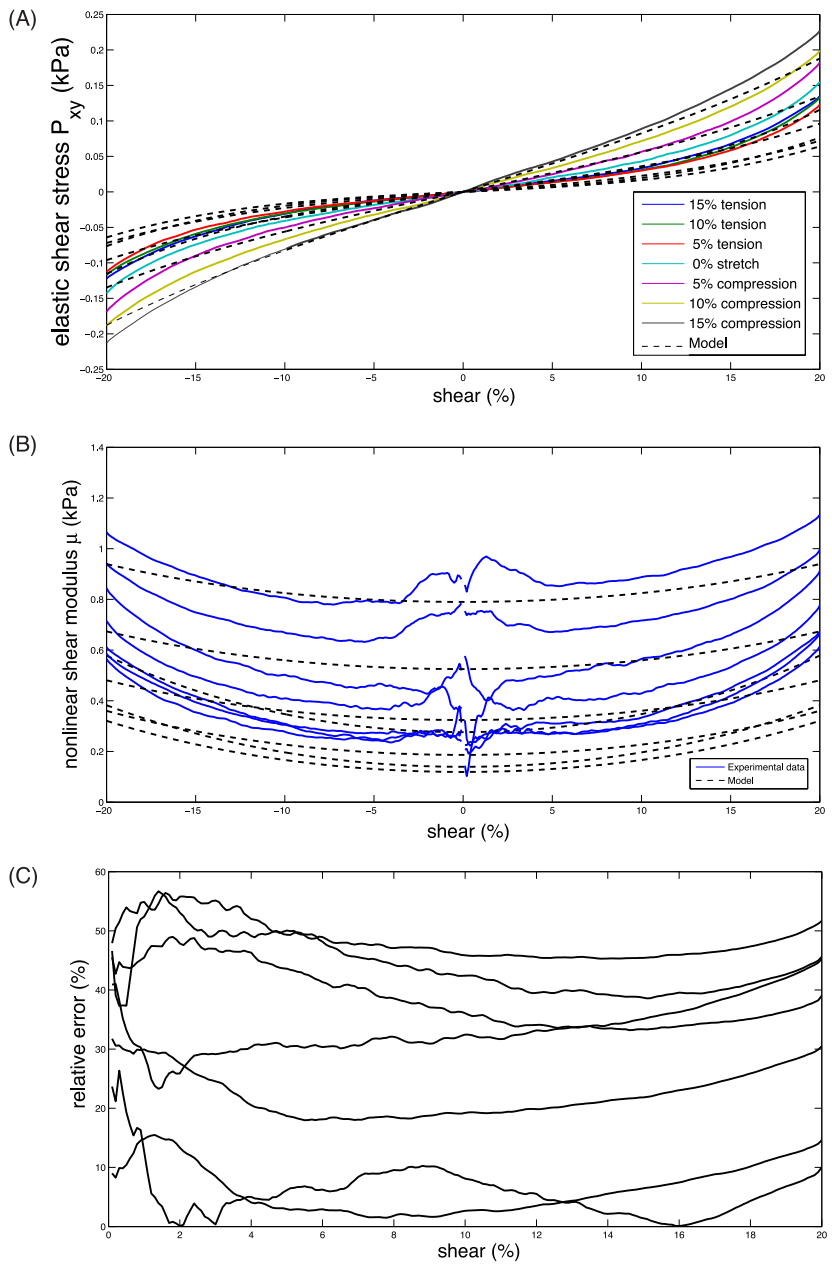

Fig. 7. Constitutive behavior of strain-energy function $\mathcal{W}$ with $c_0 = 0.0653$ kPa, $\alpha = 7.1813$, $\bar{c}_1 = -3.8201$ kPa, and $\bar{c}_2 = 3.5376$ kPa under simple shear superposed on different levels of axial tension or compression: (A) shear stress P_{xy} versus shear strain, experiment and model, (B) nonlinear shear modulus μ versus axial strain, experiment and model, and (C) associated relative error for the shear stress P_{xy}. The corresponding linear shear modulus is $\mu_0 = 0.1864$ kPa.

feasible solution and strong dependency of the optimal solutions on initialization (Ogden et al., 2004), our key observations about the particular behavior of the nonlinear shear modulus are essential in finding suitable model solutions.

Our first model consists of one Ogden-term with two parameters which are derived by a different calibration strategy than the one tested in Budday et al. (2017). Specifically, to find the two model parameters, we first identify reliable data for the nonlinear shear modulus under small shear deformations from our experimental measurements, then calibrate to these values the nonlinear shear modulus of the hyperelastic model under small shear superposed on varying axial tension or compression. We emphasize here that the preliminary step whereby we identify reliable data for the small shear range is only required because the available data are particularly noisy in that range. When reliable experimental data are provided directly, this preliminary step is not needed. In the linear elastic limit, the model parameters define a linear shear modulus

of $\mu_0 = 0.3779$ kPa, and, under the assumption of incompressibility, a Young's modulus of $E_0 = 1.1338$ kPa. The results predicted by this model are in very good agreement with all the given experimental data for simple shear superposed on different level of axial tension or compression simultaneously, especially in the small shear regime and in the linear elastic limit. However, under large shear deformations, the results are less accurate, since, as suggested by the experimental data, when compression increases, the nonlinear elastic modulus increases slower under larger shear, but when tension increases, the rate of increase in this modulus remains virtually the same for different levels of shear.

We also construct a three-term (four-parameter) Ogden-type model by systematically exploiting key findings from the available experimental data. Specifically, the multiaxial loading tests reveal that (i) the elastic response of brain tissue under varying shear superposed on different levels of tension and compression is qualitatively similar to the response under simple shear, and (ii) for a given shear superposed on varying levels of tension and compression, the elastic behavior under large shear is consistent with that under small shear. To capture these unique characteristics, we devise a three-step approach. First, we define a strain-energy function $\mathcal{W}_1$ and introduce its nonlinear shear modulus μ_1, which is a function of the deformation and represents the ratio between the shear stress and the shear. We calibrate the model parameters from the experimental data at finite deformation. Second, we correct the model by a second strain-energy function $\mathcal{W}_2$ of Mooney–Rivlin-type with the nonlinear shear modulus μ_2 and calibrate the model parameters at the small shear strain limit. Third, we add both models to obtain the overall strain-energy function $\mathcal{W} = \mathcal{W}_1 + \mathcal{W}_2$. To formalize the procedure by which we identify our parameters, we use experimental measurements for the shear stress under simple shear superposed on a chosen axial stretch and for the shear modulus under small shear superposed on varying axial tension or compression. In the linear limit, these parameters define a linear shear modulus of $\mu_0 = 0.1864$ kPa, and, under the assumption of incompressibility, a Young's modulus of $E_0 = 0.5593$ kPa. With this parameterization, our model is capable of predicting the elastic behavior of human brain tissue under combined multiaxial loading.

Our proposed models are the only hyperelastic models to date calibrated simultaneously to experimental data for brain tissue under finite simple shear superposed on varying axial tension or compression. With the advantage of a robust and systematic parameter identification, the hyperelastic models proposed here may be generalized to other soft, lipid-rich biological tissues with similar constitutive features, including liver or adipose tissue. Critically, our modeling techniques highlight the central role played by the nonlinear shear modulus to explain tissue behavior in large deformations.

Acknowledgements

The support for L. Angela Mihai by the Engineering and Physical Sciences Research Council of Great Britain under research grant EP/M011992/1 is gratefully acknowledged. This work was supported also by the German National Science Foundation grant STE 544/50 to Silvia Budday, by the Humboldt Research Award and the National Institutes of Health grant U01 HL119578 to Ellen Kuhl, and by the Timoshenko Scholar Award to Alain Goriely.

Supplementary materials

Supplementary material associated with this article can be found, in the online version, at doi:10.1016/j.jmps.2017.05.015.

Appendix A. Biomechanical testing

To characterize the mechanical response of human brain tissue under multiaxial loading, we extracted a total of four specimens of $5 \times 5 \times 5$ mm^3 from the corona radiata, the outer white matter, of three human cadavers obtained during autopsy from the local health authorities with a post mortem interval of less than 24 h. Directly after autopsy, we cut one exemplary fresh tissue slice of each human brain for biomechanical testing and comparison. The study was approved by the Ethics Commission of the Medical University of Graz, Austria, with the approval number 25–420 ex 12/13. We kept the tissue refrigerated at 3 °C and humidified with phosphate-buffered saline solution at all times to minimize tissue degradation. We tested all samples within 48 h after subject acquisition. This resulted in a total post-mortem interval between death and the end of biomechanical testing of less than 60 h. Note that the post-mortem time of up to 60 h after death could potentially affect brain tissue properties. While studies on porcine brain tissue revealed a slight increase in tissue stiffness beginning 6 h post-mortem (Garo et al., 2007), other experiments on bovine brain tissue showed no change in tissue stiffness between 2 h and 5 days post mortem (Budday et al., 2015). Within the time window between the first and last sample tested, we could not observe a notable change in tissue stiffness. We mounted each specimen onto the custom-designed triaxial testing device (Sommer et al., 2013) to apply combined shear and compression or tension loadings. The system operates with a stroke resolution of 0.04 µm in the y-direction and with a stroke resolution of 0.25 µm in the x- and z-directions. We achieved motor control and data acquisition using the software testXpert II Version 3.2 (Zwick/Roell GmbH & Co. KG, Ulm, Germany) on a Windows-based personal computer. We conducted all tests at room temperature and chose quasi-static loading conditions with a speed of 2 mm/min. We first increased the compressive strain from 0% to 25% in increments of 5%, and subsequently the tensile strain from 5% to 25%, also in increments of 5%, by moving the upper platform in the y-direction. This resulted in axial stretches of $a = (L_y + \Delta y)/L_y$ with a y-displacement Δy and a specimen height L_y. At each axial stretch level, we applied a sinusoidal simple shear up to a shear strain $\gamma = ka = 0.2$ in the x- and z-directions, where the shear strain γ specifies the relative in-plane displacement of two parallel layers in the material

body divided by their separation distance L_y. During shear loading, the lower platform moved relative to the fixed upper platform using a biaxial translation stage with the maximum displacements $\Delta x = \Delta z = 0.2L_y$. We applied three cycles of shear per stretch level and direction, where two cycles served as preconditioning steps and the third cycle was used for data analysis (see Supplementary Material). We recorded the forces with a three-axe force-sensor (K3D40, ME-Measuring Equipment, Henningsdorf, Germany) and calculated the shear stresses $P_{xy} = f/A$ and $P_{yz} = f/A$ as the shear force f, the force recorded in the direction of shear, divided by the shear area $A = L_xL_z$ with the specimen length L_x and specimen width L_z. The "elastic" responses which we use for calibrating the hyperelastic constitutive model parameters were obtained as the average between the loading and unloading responses. For further discussions on the effects of post-mortem time and sample preparation, as well as on the limitations of in vitro testing and the methods used to extract elastic properties, we refer to Budday et al. (2017).

Appendix B. Preliminary approximation of experimental data

Given all the data sets for simple shear, up to 20%, combined with different compression or tension loading, up to 25% tension or compression (in 5% increments), we can calibrate the model $\mathcal{W}_{\text{og}}$ defined by (17) for each prescribed stretch a, as in Budday et al. (2017). Figs. B.8 and B.9 show the constitutive behavior of the strain-energy function $\mathcal{W}_{\text{og}}$ of Eq. (17) in terms of the shear stress P_{xy} versus shear strain, the nonlinear shear modulus $\mu = P_{xy}/ka$, and the relative error $|P_{xy}^{\text{model}} - P_{xy}^{\text{data}}|/|P_{xy}^{\text{data}}|$, where P_{xy}^{model} and P_{xy}^{data} represent the predicted and measured values of the shear stress, respectively, and $|\cdot|$ denotes the absolute value. These figures also suggest that some of the collected data are inaccurate, as discontinuities and noise appear in the nonlinear shear modulus at less than 5% shear strain. Note that, since the discontinuities and the noise are in the gradient, they are not captured by the plots of the measured shear stress. Nevertheless, we can still calibrate the function $\mathcal{W}_{\text{og}}$ to the correct experimental data, which leads to a very accurate approximation at over 5% shear, and consider the values of the shear stress and nonlinear shear modulus identified by the calibrated model as reliable predictions of the elastic behavior in both the small and the large shear regime. In particular, for each axial stretch a, the nonlinear shear modulus under small shear $\widetilde{\mu}(a)$ is given by (20), which for the purpose of this study we refer to as $\widetilde{\mu}_{data}(a)$.

In the linear elastic limit, the shear modulus (21) identified for the model calibrated to the simple shear data, i.e., $\mathcal{W}_{\text{og}}$ with parameters $c_0 = -0.0297$ kPa and $\alpha = -11.3757$, is equal to $\mu_0 = c_0\alpha = 0.3379$ kPa. However, if we consider the strain energy function $\mathcal{W}_{\text{og}}$ calibrated to the experimental data for simple shear and apply axial tension or compression followed by simple shear to this model, we find that the approximation of the experimental data corresponding to simple shear superposed on axial compression becomes less and less accurate as compression increases, even though the approximation of the data for simple shear superposed on axial tension is reasonable (see Fig. B.10).

In Mangan et al. (2016), a hyperelastic model calibrated to experimental data for porcine brain tissue subject to simple shear was proposed, whereby the shear stress increases linearly with respect to the shear parameter $0 \leq K \leq 1$, as also shown experimentally by Rashid et al. (2013). A careful inspection of the experimental data in Mangan et al. (2016) and Rashid et al. (2013) suggests that there are 3–5 non-zero test data supplied for simple shear with shear parameter $0 \leq K \leq 0.2$, corresponding to 0%–20% shear strain. Our experimental tests for human brain tissue provide 201 data values for simple shear from 0% to 20% shear strain (see top-left-hand plot in Fig. B.8, or equivalently top left-hand plot in Fig. B.9), and similarly, 401 data for every simple shear deformation superposed on up to 25% tension or compression, in 5% increments, i.e., 401 $\times$ 11 data values in total. More importantly, while the tests in Mangan et al. (2016); Rashid et al. (2013) were carried out without pre-conditioning and at high strain rates (30/s or higher, requiring velocities of over 120 mm/s), the experimental measurements for our study were taken under quasi-static loading (with velocity of 2 mm/min), and averaged between the loading and unloading paths (see Appendix A). For human brain tissue, in Shuck and Advani (1972), a linear behaviour compatible with a Neo–Hookean model was found under small torsion, up to 3.5% strain. The linear behaviour of both porcine and human brain tissue in shear was also observed in Moran et al. (2014) and Nicolle et al. (2004), where Ogden models were proposed for large deformations. Softening in shear was noted by Hrapko et al. (2008), Jin et al. (2013), Pogoda et al. (2014) and Prange and Margulies (2002). By contrast, stiffening in shear was reported in Budday et al. (2017), Darvish and Crandall (2001) and Donnelly and Medige (1997). Furthermore, in Darvish and Crandall (2001), the discrepancies observed in the mechanical properties of brain tissue in other studies were shown to be related to the strain conditioning effect, consisting in non-recoverable changes in the material properties under finite strains, which also make the mechanical responses of the tissue almost isotropic.

Table B.3 summarizes the above mentioned publications, where experimental results under shear or combined stretch and shear deformations of brain tissues were reported. From this table, we see that there are wide variations in the conditions of measurement, particularly those reported by different authors. Besides, the data which many authors provide to calibrate hyperelastic models are rather sparse, and the table clearly demonstrates that the data set which we analyse here is the most extensive and the only one for brain tissue in finite multiaxial loading. This precludes conclusive quantitative comparisons between independent results (Chatelin et al., 2010), and makes mathematical modeling of this tissue extremely challenging. Nevertheless, it can reasonably be inferred that, when brain tissue is subject to large strains, the shear stress increases strongly under axial compression, regardless of the stress-strain response due to shear deformation alone (Budday et al., 2017; Pogoda et al., 2014).

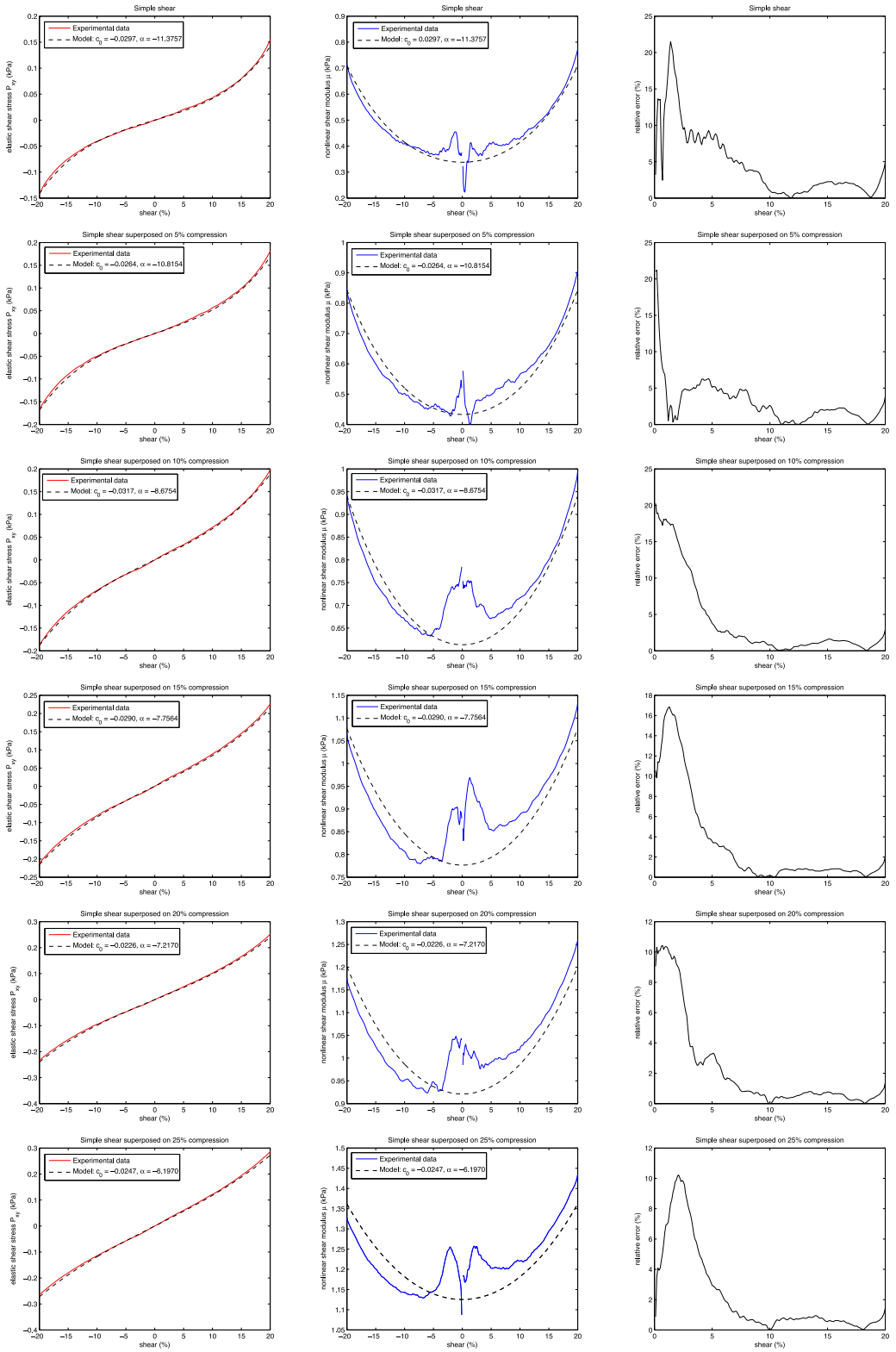

Fig. B8. Shear stress P_{xy} and nonlinear shear modulus μ versus shear strain predicted by the hyperelastic model $\mathcal{W}_{\text{og}} = c_0(a)\left(\lambda_1^{2\alpha(a)} + \lambda_2^{2\alpha(a)} + \lambda_3^{2\alpha(a)} - 3\right)/(2\alpha(a))$ with (black dashed curve) compared to individual data sets (colored continuous line) for simple shear and for simple shear superposed on different axial deformations, and relative errors for the shear stress P_{xy}, for simple shear and simple shear superposed on different axial compressions.

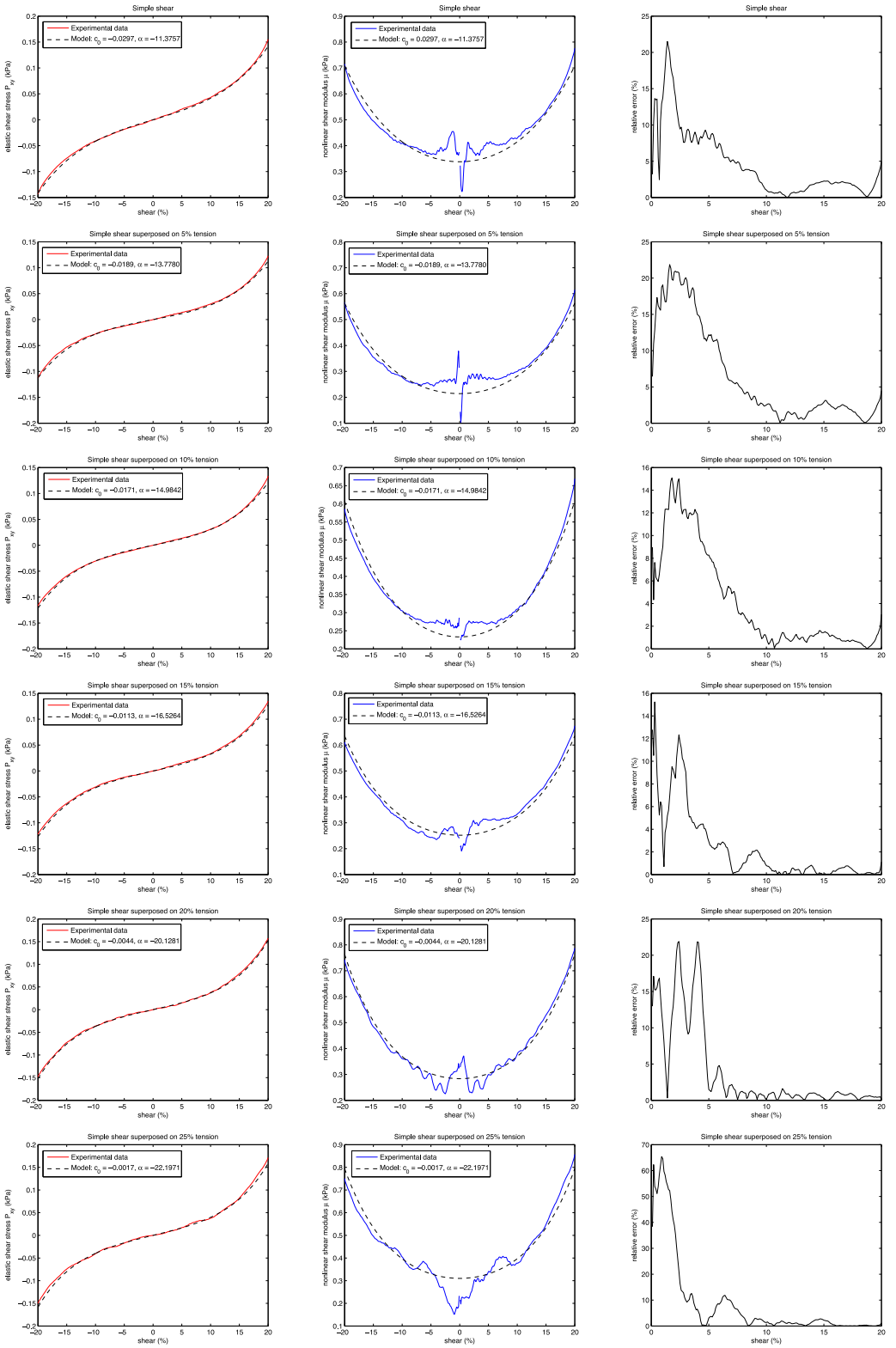

Fig. B9. Shear stress P_{xy} and nonlinear shear modulus μ versus shear strain predicted by the hyperelastic model $\mathcal{W}_{\rm og} = c_0(a)\big(\lambda_1^{2\alpha(a)} + \lambda_2^{2\alpha(a)} + \lambda_3^{2\alpha(a)} - 3\big)/(2\alpha(a))$ with (black dashed line) compared to individual data sets (colored continuous curve) for simple shear and for simple shear superposed on different axial deformations, and relative errors for the shear stress P_{xy}, for simple shear and for simple shear superposed on different axial tensions.

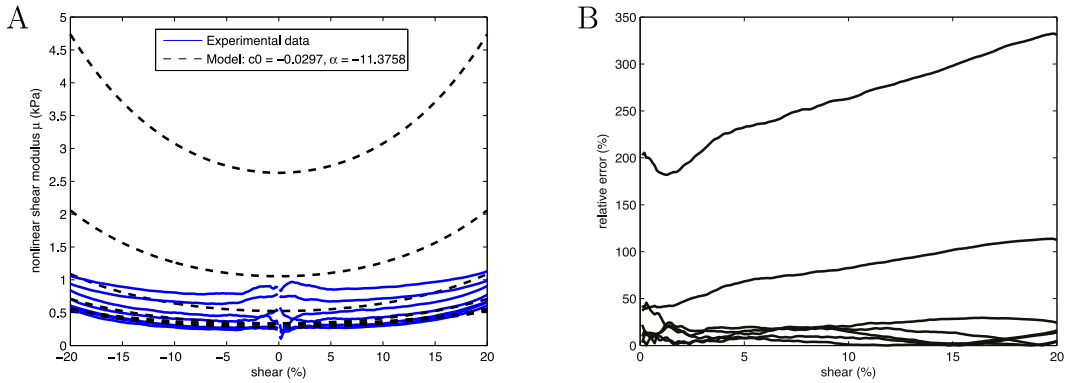

Fig. B10. Constitutive behavior of strain-energy function $\mathcal{W}_{og} = c_0(a)\left(\lambda_1^{2\alpha(a)} + \lambda_2^{2\alpha(a)} + \lambda_3^{2\alpha(a)} - 3\right)/(2\alpha(a))$ with parameters $c_0 = -0.0297$ kPa and $\alpha = -11.3757$ under simple shear superposed on up to 15% axial tension or compression: (A) nonlinear shear modulus μ versus axial strain, given data and model, and (B) associated relative error for the shear stress P_{xy}.

Table B3
Publications where experimental results for brain tissue under shear were reported, with the conditions of measurement and number of test data available for model calibration specified.

tissue	temperature	deformation	strain rate	strain range	data	reference
human brain	room	shear	dynamic loading	0%–100%	–	Donnelly and Medige (1997)
human brain	body 37 °C	shear	dynamic loading	0%–50%	11	Jin et al. (2013)
porcine brain	room 22–23 °C	shear	dynamic loading	0%–100%	20	Rashid et al. (2013)
porcine brain	room 23 °C	shear superposed on compression	dynamic loading	0%–10% shear −10% axial	7	Hrapko et al. (2008)
bovine brain	body 37 °C	shear	dynamic loading/unloading	0%–20%	–	Darvish and Crandall (2001)
human brain	–	shear	quasi-static loading	0%–50%	8	Prange and Margulies (2002)
porcine brain	–	shear	quasi-static loading	0%–50%	8	Prange and Margulies (2002)
mouse brain	room/body 23 °C/37 °C	shear superposed on compression	quasi-static loading	0%–45% shear −40%–0% axial	10 × 2	Pogoda et al. (2014)
mouse brain	–	shear superposed on tension/compression	quasi-static loading	2% shear −40%–40% axial	9	Pogoda et al. (2014)
human brain	room	shear superposed on tension/compression	quasi-static loading/unloading	−20%–20% shear −25%–25% axial	401 × 11	Budday et al. (2017)

Appendix C. Three-term (three-parameter) constitutive model

In this appendix, at Step 2 in Section 4, we consider the three-term (three-parameter) Ogden model

$$\begin{aligned}\mathcal{W}_3(\lambda_1,\lambda_2,\lambda_3) =& \frac{c_1}{2}\left(\lambda_1^2+\lambda_2^2+\lambda_3^2-3\right)\\ &+\frac{c_2}{2}\left(\lambda_1^{-2}+\lambda_2^{-2}+\lambda_3^{-2}-3\right)\\ &+\frac{c_3}{4}\left(\lambda_1^4+\lambda_2^4+\lambda_3^4-3\right),\end{aligned} \tag{C.1}$$

with the constant parameters c_i, $i = 1, 2, 3$, instead of the one-term (two-parameter) hyperelastic model (22). For the three-term model, the nonlinear shear modulus (11), the nonlinear shear modulus under small shear strain (15), and their linear elastic limit (16) take on the following explicit forms

$$\mu(a,k) = c_1 + \frac{c_2}{a} + c_3\left(\lambda_1^2+\lambda_2^2\right), \tag{C.2}$$

$$\widetilde{\mu}(a) = \lim_{k\to 0}\mu(a,k) = c_1 + \frac{c_2}{a} + c_3\frac{1+a^3}{a}, \tag{C.3}$$

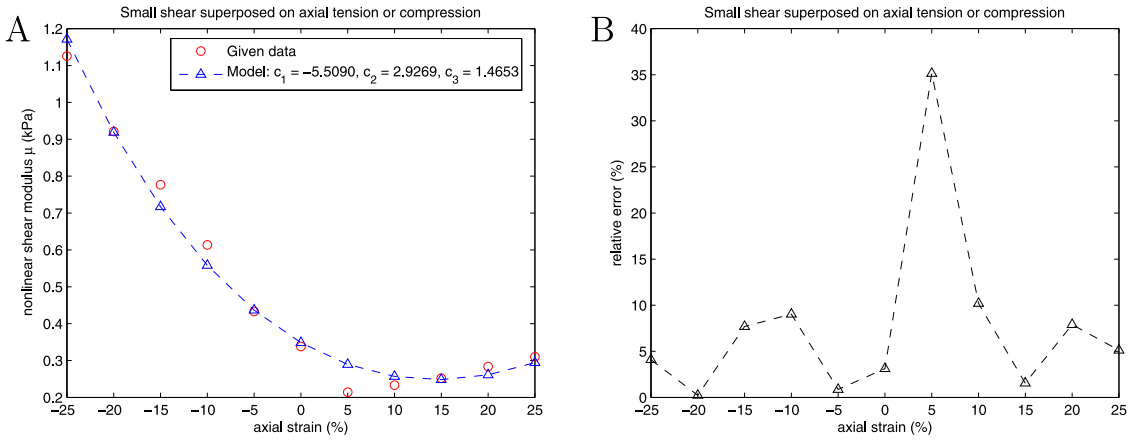

Fig. C11. Constitutive behavior of strain-energy function $\mathcal{W}_3 = c_1\big(\lambda_1^2+\lambda_2^2+\lambda_3^2-3\big)/2 + c_2\big(\lambda_1^{-2}+\lambda_2^{-2}+\lambda_3^{-2}-3\big)/2 + c_3\big(\lambda_1^4+\lambda_2^4+\lambda_3^4-3\big)/4$ with parameters $c_1 = -5.5090$ kPa, $c_2 = 2.9269$ kPa, and $c_3 = 1.4653$ kPa under small shear superposed on axial tension or compression: (A) nonlinear shear modulus $\widetilde{\mu}$ versus axial strain, given data and model, and (B) associated relative error for the shear stress P_{xy}.

Table C4
Strain-energy function with related model parameters and calibrated values (and units) for human brain tissues.

strain energy	eq.	model	parameter	value	unit
$\mathcal{W}_3$	(C.1)	Ogden	c_1	−5.5090	kPa
			c_2	2.9269	kPa
			c_3	1.4653	kPa
linear elastic limit	(C.4)	–	μ_0	0.3485	kPa

$$\widetilde{\mu}_0 = \lim_{a\to 1}\widetilde{\mu}(a) = c_1 + c_2 + 2c_3. \tag{C.4}$$

To derive the model parameters, we calibrate the nonlinear shear modulus $\widetilde{\mu}(a)$ of Eq. (C.3) to the known values $\widetilde{\mu}_{data}(a)$ identified at the preliminary Step 1 in Section 4 (see also Appendix B), for small shear superposed on up to 25% tension or compression (in 5% increments), and obtain $c_1 = -5.5090$ kPa, $c_2 = 2.9269$ kPa, and $c_3 = 1.4653$ kPa. This calibration is illustrated in Fig. C.11 together with the associated relative error $|P_{xy}^{\text{model}} - P_{xy}^{\text{data}}|/|P_{xy}^{\text{data}}|$. A quick comparison with the relative errors shown in Fig. 3C suggests that this three parameter model (C.1) offers a slightly closer match to the given data for small shear superposed on varying tension or compression than the two parameter model (22).

This model predicts a linear shear modulus (C.4) of $\mu_0 = 0.3485$ kPa and a Young's modulus of $E_0 = 3\mu_0 = 1.0455$ kPa. Thus the three parameter model (C.1) produces a slightly more accurate approximation to the linear shear modulus $\mu_0 = 0.3379$ kPa identified at Step 1 (see Appendix B) than the two parameter model (22).

Table C.4 summarizes the strain-energy function for this hyperelastic model, its constant parameters, their calibrated values, and units. Fig. C.12 summarizes the predicted shear stress P_{xy} and nonlinear shear modulus μ compared to the experimental data sets for simple shear, up to 20% shear strain, superposed on up to 25% compression or tension (in 5% increments), and the relative errors. A comparison with Fig. 4 further suggests that, in large shear also, the results predicted by the three-parameter model (C.1) are closer to the given data than those predicted by the two parameter model (22). However, the decrease in the relative errors shown in Fig. C.12C compared to those in Fig. 4C is limited, especially at more than 10% shear. This trend was also observed when the number of Ogden terms was further increased, even though the approximation under small shear superposed on varying axial stretch continued to improve, as discussed in Mihai et al. (2015) (results not shown).

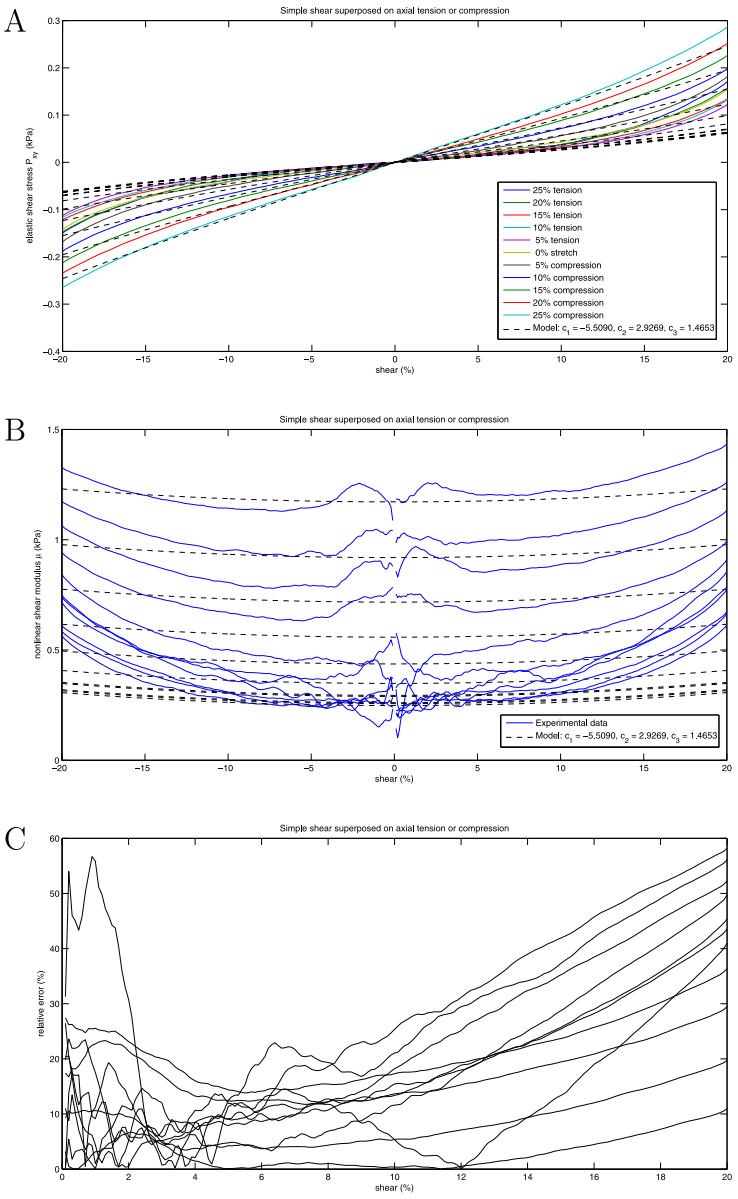

Fig. C12. Constitutive behavior of strain-energy function $\mathcal{W}_3 = c_1\left(\lambda_1^2+\lambda_2^2+\lambda_3^2-3\right)/2 + c_2\left(\lambda_1^{-2}+\lambda_2^{-2}+\lambda_3^{-2}-3\right)/2 + c_3\left(\lambda_1^4+\lambda_2^4+\lambda_3^4-3\right)/4$ with parameters $c_1 = -5.5090$ kPa, $c_2 = 2.9269$ kPa, and $c_3 = 1.4653$ kPa under simple shear superposed on different levels of axial tension or compression: (A) shear stress P_{xy} versus shear strain, experiment and model, (B) nonlinear shear modulus μ versus axial strain, experiment and model, and (C) associated relative error for the shear stress P_{xy}. The corresponding linear shear modulus is $\mu_0 = 0.3438$ kPa.

References

Bayly, P.V., Black, E.E., Pedersen, R.C., Leister, E.P., Genin, G.M., 2006. In vivo imaging of rapid deformation and strain in an animal model of traumatic brain injury. J. Biomech. 39, 1086–1095.

Beatty, M.F., 1996. Introduction to nonlinear elasticity. In: Carroll, M.M., Hayes, M.A. (Eds.), Nonlinear Effects in Fluids and Solids. Plenum Press, New York and London, pp. 13–104.

Budday, S., Nay, R., de Rooij, R., Steinmann, P., Wyrobek, T., Ovaert, T.C., Kuhl, E., 2015. Mechanical properties of gray and white matter brain tissue by indentation. J. Mech. Behav. Biomed. Mater. 46, 318–330.

Budday, S., Sommer, G., Birkl, C., Langkammer, C., Haybäck, J., Kohnert, J., Bauer, M., Paulsen, F., Steinmann, P., Kuhl, E., Holzapfel, G.A., 2017. Mechanical characterization of human brain tissue. Acta Biomaterialia 48, 319–340.

Chatelin, S., Constantinesco, A., Willinger, R., 2010. Fifty years of brain tissue mechanical testing: from in vitro to in vivo investigations. Biorheology 47, 255–276. PubMed: 21403381

Cloots, R.J.H., van Dommelen, J.A.W., Nyberg, T., Kleiven, S., Geers, M.D.G., 2011. Micromechanics of diffuse axonal injury: influence of axonal orientation and anisotropy. Biomech. Model. Mechanobiol. 10, 413–422.

Comley, K.S.C., Fleck, N.A., 2012. The compressive response of porcine adipose tissue from low to high strain rate. Int. J. Impact Eng. 46, 1–10.

Darvish, K.K., Crandall, J.R., 2001. Nonlinear viscoelastic effects in oscillatory shear deformation of brain tissue. Med. Eng. Phys. 23, 633–645.
Destrade, M., Gilchrist, M.D., Murphy, J.G., Rashid, B., Saccomandi, G., 2015. Extreme softness of brain matter in simple shear. Int. J. Non–Linear Mech. 75, 54–58.
Destrade, M., Murphy, J.G., Saccomandi, G., 2012. Simple shear is not so simple. Int. J. Non-Linear Mech. 47, 210–214.
Donnelly, B.R., Medige, J., 1997. Shear properties of human brain tissue. J. Biomech. Eng. 119, 423–432.
Franceschini, G., Bigoni, D., Regitnig, P., Holzapfel, G.A., 2006. Brain tissue deforms similarly to filled elastomers and follows consolidation theory. J. Mech. Phys. Solids 54, 2592–2620.
Garo, A., Hrapko, M., Van Dommelen, J.A.W., Peters, G.W.M., 2007. Towards a reliable characterisation of the mechanical behaviour of brain tissue: the effects of post-mortem time and sample preparation. Biorheology 44, 51–58.
Goriely, A., Budday, S., Kuhl, E., 2015a. Neuromechanics: from neurons to brain. Adv. Appl. Mech. 48, 79–139.
Goriely, A., Geers, M.G.D., Holzapfel, G.A., Jayamohan, J., Jerusalem, A., Sivaloganathan, S., Squier, W., van Dommelen, J.A.W., Waters, S., Kuhl, E., 2015b. Mechanics of the brain: perspectives, challenges, and opportunities. Biomech. Model. Mechanobiol. 14, 931–965.
Holzapfel, G.A., 2000. Nonlinear Solid Mechanics: A Continuum Approach for Engineering. John Wiley & Sons.
Holzapfel, G.A., Gasser, T.C., Ogden, R.W., 2000. A new constitutive framework for arterial wall mechanics and a comparative study of material models. J. Elast. Phys. Sci. Solids 61, 1–48.
Horgan, C.O., Saccomandi, G., 2003. A description of arterial wall mechanics using limiting chain extensibility constitutive models. Biomech. Model. Mechanobiol. 1, 251–266.
Hrapko, M., van Dommelen, J.A.W., Peters, G.W.M., Wismans, J.S.H.M., 2008. Characterisation of the mechanical behaviour of brain tissue in compression and shear. Biorheology 45, 663–676.
Jin, X., Zhu, F., Mao, H., Shen, M., Yang, K.H., 2013. A comprehensive experimental study on material properties of human brain tissue. J. Biomech. 46, 2795–2801.
Levental, I., Georges, P.C., Janmey, P.A., 2007. Soft biological materials and their impact on cell function. Soft Matter 3, 299–306.
Mangan, R., Destrade, M., Saccomandi, G., 2016. Strain energy function for isotropic non-linear elastic incompressible solids with linear finite strain response in shear and torsion. Extreme Mech. Lett. 9, 204–206.
Mihai, L.A., Chin, L.K., Janmey, P.A., Goriely, A., 2015. A comparison of hyperelastic constitutive models applicable to brain and fat tissues. J. R. Soc. Interface 12. 20150486
Mihai, L.A., Goriely, A., 2011. Positive or negative Poynting effect? The role of adscititious inequalities in hyperelastic materials. Proc. R. Soc. A 467, 3633–3646.
Mihai, L.A., Goriely, A., 2013. Numerical simulation of shear and the Poynting effects by the finite element method: an application of the generalised empirical inequalities in non-linear elasticity. Int. J. Non-Linear Mech. 49, 1–14.
Miller, K., Chinzei, K., 1997. Constitutive modelling of brain tissue: experiment and theory. J. Biomech. 30, 1115–1121.
Miller, K., Chinzei, K., 2002. Mechanical properties of brain tissue in tension. J. Biomech. 35, 483–490.
Misra, S., Ramesh, K.T., Okamura, A.M., 2010. Modelling of non-linear elastic tissues for surgical simulation. Comput. Methods Biomech. Biomed. Eng. 13, 811–818.
Mooney, M., 1940. A theory of large elastic deformation. J. Appl. Phys. 11, 582–592.
Moran, R., Smith, J.H., Garćia, J.J., 2014. Fitted hyperelastic parameters for human brain tissue from reported tension, compression, and shear tests. J. Biomech. 47, 3762–3766.
Nicolle, S., Lounis, M., Willinger, R., 2004. Shear properties of brain tissue over a frequency range relevant for automotive impact situations: new experimental results. Stapp Car Crash J. 48, 239–258.
Ogden, R.W., 1972. Large deformation isotropic elasticity II: on the correlation of theory and experiment for incompressible rubberlike solids. Proc. R. Soc. A 326, 565–584.
Ogden, R.W., 1997. Non-Linear Elastic Deformations. Dover, New York.
Ogden, R.W., Saccomandi, G., Sgura, I., 2004. Fitting hyperelastic models to experimental data. Comput. Mech. 34 (6), 484–502.
Pogoda, K., Chin, L.K., Georges, P.C., Byfield, F.R.G., Bucki, R., Kim, R., Weaver, M., Wells, R.G., Marcinkiewicz, C., Janmey, P.A., 2014. Compression stiffening of brain and its effect on mechanosensing by glioma cells. New J. Phys. 16. 075002
Prange, M.T., Margulies, S.S., 2002. Regional, directional, and age-dependent properties of the brain undergoing large deformation. J. Biomech. Eng. 124, 244–252.
Rajagopal, K.R., Wineman, A.S., 1987. New universal relations for nonlinear isotropic elastic materials. J. Elast. 17, 75–83.
Rashid, B., Destrade, M., Gilchrist, M.D., 2012. Mechanical characterization of brain tissue in compression at dynamic strain rates. J. Mech. Behav. Biomed. Mater. 10, 23–38.
Rashid, B., Destrade, M., Gilchrist, M.D., 2013. Mechanical characterization of brain tissue in simple shear at dynamic strain rates. J. Mech. Behav. Biomed. Mater. 28, 71–85.
Rashid, B., Destrade, M., Gilchrist, M.D., 2014. Mechanical characterization of brain tissue in tension at dynamic strain rates. J. Mech. Behav. Biomed. Mater. 33, 43–54.
Rivlin, R.S., 1948. Large elastic deformations of isotropic materials. IV. Further developments of the general theory. Philos. Trans. R. Soc. London A 241, 379–397.
de Rooij, R., Kuhl, E., 2016. Constitutive modeling of brain tissue: current perspectives. Appl. Mech. Rev. 68. 010801
Shuck, L.Z., Advani, S.H., 1972. Rheological response of human brain tissue in shear. J. Basic Eng. 94, 905–911.
Sommer, G., Eder, M., Kovacs, L., Pathak, H., Bonitz, L., Mueller, C., Regitnig, P., Holzapfel, G.A., 2013. Multiaxial mechanical properties and constitutive modeling of human adipose tissue: a basis for preoperative simulations in plastic and reconstructive surgery. Acta Biomaterialia 9, 9036–9048.
Truesdell, C., Noll, W., 2004. The Non-Linear Field Theories of Mechanics, 3rd ed Springer, New York.